DFT investigation of the effect of spin-orbit coupling on the NMR shifts in paramagnetic solids

Roberta Pigliapochi, Andrew J. Pell, Ieuan D. Seymour, Clare P. Grey, Davide Ceresoli, and Martin Kaupp

Phys. Rev. B **95**, 054412 — Published 8 February 2017

DOI: 10.1103/PhysRevB.95.054412

DFT investigation of the effect of spin-orbit coupling on the NMR shifts in paramagnetic solids

Roberta Pigliapochi, Andrew J. Pell,* Ieuan D. Seymour, and Clare P. Grey†
Department of Chemistry, University of Cambridge, Lensfield Road, CB2 1EW Cambridge, UK

Davide Ceresoli
CNR-ISTM, Universitá degli studi di Milano, via Golgi 19, 20133 Milano, Italy

Martin Kaupp
Institut für Chemie, Technische Universität Berlin, Strasse des 17. Juni 135, 10623 Berlin, Germany
(Dated: January 12, 2017)

Nuclear Magnetic Resonance (NMR) spectroscopy is a powerful tool for studying the structural and electronic properties of paramagnetic solids. However, the interpretation of paramagnetic NMR spectra is often challenging as a result of the interactions of unpaired electrons with the nuclear spins of interest. In this work, we extend the formalism of the paramagnetic NMR shielding in the presence of spin-orbit coupling towards solid systems with multiple paramagnetic centres. We demonstrate how the single-ion Electron Paramagnetic Resonance (EPR) g-tensor is defined and calculated in periodic paramagnetic solids. We then calculate the hyperfine tensor and the g-tensor with density functional theory (DFT) to show the validity of the presented model and we further demonstrate how these interactions can be combined to give the overall paramagnetic shielding tensor, $\boldsymbol{\sigma}^s$. The method is applied to a series of olivine-type $LiTMPO_4$ materials (with TM=Mn, Fe, Co and Ni) and the corresponding ^{7}Li and ^{31}P NMR spectra are simulated. We analyse the effects of spin-orbit coupling and of the electron-nuclear magnetic interactions on the calculated NMR parameters. A detailed comparison is presented between contact and dipolar interactions across the $LiTMPO_4$ series, in which the magnitudes and signs of the non-relativistic and relativistic components of the overall isotropic shift and shift anisotropy are computed and rationalized.

I. INTRODUCTION

Materials containing paramagnetic centres with unpaired electron spins, such as transition metal (TM) ions, are widely used in the fields of biochemistry [1, 2], catalysis [3–5], and electrochemistry [6–8]. Nuclear Magnetic Resonance (NMR) spectroscopy is a powerful technique for analysing the local structure in paramagnetic solids, as the unpaired electrons of the TM ions induce a paramagnetic shift and shift anisotropy that provide detailed information concerning the structural and chemical environment of the NMR observed centre (OC) [9–13]. However, the interpretation of these spectra proves very challenging, as the presence of the paramagnetic centres results in multiple effects on the observed NMR lineshapes [14–17]. The through-bond transfer of unpaired-electron spin density onto the nuclear position of the OC induces a so-called Fermi contact shift, which is a direct measure of the electronic structure of the TM, the electronic spin transfer through the TM-O-OC bond and the degree of interaction between the relevant orbitals [18]. The through-space hyperfine dipolar interaction between the magnetic moments of the unpaired-electron spin density and that of the observed nucleus results in a significant broadening of the spectrum. In the presence of spin-orbit coupling, the deviation of the g-tensor from the free-electron g-factor, known as the g-shift, modifies both the Fermi-contact and dipolar contributions to the shift. In particular, the combination of the anisotropy of the g-tensor and the zero-field splitting interaction with the dipolar coupling lead to a through-space contribution to the paramagnetic shift, referred to as pseudo-contact shift. The spin-orbit correction to the Fermi contact term *via* the isotropic g-shift also adds a contribution to the NMR shift. All these terms depend on the electronic structure of the TM. The pseudo-contact term depends on the distance between the OC and the paramagnetic centre(s), and on the relative orientation of the g- and hyperfine tensors, and the contact term depends on the through-bond transfer of unpaired electron density to the OC. In addition, the coupling between the g-shift and the hyperfine dipolar tensor modifies the NMR shift anisotropy. To help with the often challenging interpretation of the paramagnetic NMR spectra, first-principles quantum-mechanical studies can provide detailed insight at the atomic and electronic level. Substantial progress has been made in the theoretical description of various contributions to the NMR shift of molecular systems with a single paramagnetic centre. After the pioneering work of Kurland and McGarvey [16], Moon and Patchkovski derived a formalism to describe the entire shift tensor including the effects of spin-orbit coupling [19], later ex-

* Current Address: Department of Materials and Environmental Chemistry, Stockholm University, Svante Arrhenius Väg 16 C, SE-106 91 Stockholm, Sweden
† Corresponding Author: cpg27@cam.ac.uk

tended to the presence of zero-field splitting by Vaara *et al.* [20, 21] and Soncini and Van den Heuvel [22], with the consequent extensive study of the NMR shift of paramagnetic molecules [23–28]. The shift mechanisms in paramagnetic transition metal-containing extended solids have been studied by Carlier, Grey and co-workers and the effects of multiple paramagnetic centres on the isotropic Fermi contact shift and its relation to the bulk magnetic properties of the solid have been qualitatively [13], and subsequently more quantitatively [29], rationalised. In their work the spin-orbit coupling effects on the NMR shift are included in an empirical effective magnetic moment. The explicit inclusion of the g-tensor in the description of the NMR spectrum is less extensively formulated for solid systems, and has mainly been presented for isolated paramagnetic centres [23, 25, 27], with only a preliminary study on paramagnetic networks [30]. This work extends the current methodology to include a description of the g-tensor in solids with multiple TM centres, and to investigate the resulting effects of spin-orbit coupling on the NMR spectra of periodic solids, which is of central importance in the analysis of many technologically relevant systems, such as battery materials. An analysis of the g- and hyperfine tensors in periodic solids is presented. A model for the derivation of the paramagnetic shielding is described, that allows the separation of the contributions to the isotropic shift and shift anisotropy. The method is applied to the investigation of the ^{7}Li and ^{31}P NMR shifts of olivine-type $LiTMPO_4$ (TM=Mn, Fe, Co and Ni). These materials, and in particular $LiFePO_4$ [31] and its Mn-substituted derivatives [32], are commercially relevant lithium-ion battery positive electrode (cathode) materials. Computational results from solid-state Density Functional Theory (DFT) are compared to the experimental shifts obtained for the corresponding powder samples [33, 34] and a method to extract individual g-tensors in solids containing high concentration of paramagnetic centres from DFT calculations is demonstrated.

II. THEORY

In paramagnetic systems, the coupling between the nuclear magnetic moment of the OC and the average spin magnetic moment of the unpaired electrons results in the paramagnetic shielding tensor, $\boldsymbol{\sigma}^s$. [35] In the presence of a single paramagnetic centre, the specific form of $\boldsymbol{\sigma}^s$ is derived to be [17, 19, 20]

$$\boldsymbol{\sigma}^s \;=\; -\frac{\mu_B\; S(S+1)}{3\;\hbar\;\gamma_N\;K_B\;T}\;\boldsymbol{g}\;\cdot\;\boldsymbol{A} \tag{1}$$

where the general form of the hyperfine tensor (up to second-order perturbation theory), $\boldsymbol{A}$, and the g-tensor, $\boldsymbol{g}$, are [17]

$$\begin{aligned}\boldsymbol{A} &= (A^{\mathrm{FC}} + A^{\mathrm{FC},2})\mathbf{1} + \boldsymbol{A}^{\mathrm{dip}} + \boldsymbol{A}^{\mathrm{dip},2}\\ \boldsymbol{g} &= (g_e + \Delta g^{\mathrm{iso}})\mathbf{1} + \boldsymbol{\Delta\tilde{g}}\end{aligned} \tag{2}$$

In eq. 1, μ_B is the Bohr magneton, S the electronic spin quantum number, $\hbar$ the reduced Planck constant, γ_N the gyromagnetic ratio of the observed nucleus, K_B the Boltzmann's constant and T the absolute temperature. The complete form of the shielding tensor includes also the orbital component that is typically approximated to the shift measured for an analogous diamagnetic system [17]. In eq. 2, the hyperfine tensor is expanded as the non-relativistic Fermi contact and dipolar contributions ($A^{\mathrm{FC}}\mathbf{1} + \boldsymbol{A}^{\mathrm{dip}}$) and the relativistic spin-orbit isotropic and dipolar terms, ($A^{\mathrm{FC},2}\mathbf{1} + \boldsymbol{A}^{\mathrm{dip},2}$). A^{FC} depends on the unpaired-electron spin density delocalized or polarized into the OC, whereas $\boldsymbol{A}^{\mathrm{dip}}$ accounts for the through-space dipolar interaction between the magnetic moment of the unpaired-electron spin density and the nuclear magnetic moment of the OC. The g-tensor in eq. 2 breaks down as g_e, the non-relativistic free-electron g value (2.002319), and $\Delta g^{\mathrm{iso}}\mathbf{1} + \boldsymbol{\Delta\tilde{g}}$, the relativistic isotropic and anisotropic parts of the g-shift tensor $\boldsymbol{\Delta g}$. The overall $\boldsymbol{\Delta g}$ corresponds to the deviation from the g_e as a consequence of the spin-orbit coupling on the paramagnetic centre when the electronic structure has a non-zero orbital angular momentum, or on heavy atoms with some fraction of unpaired-electron spin density. The individual cross terms contributing to the paramagnetic shielding tensor can be shown by substituting in eq. 1 the expressions for $\boldsymbol{A}$ and $\boldsymbol{g}$ in eq. 2. As discussed in Ref. 20, by retaining only the terms that contain at most one leading-order spin-orbit coupling term in the product $\boldsymbol{g}\cdot\boldsymbol{A}$, the resulting contributions can be separated based on the nature of the involved hyperfine term. This corresponds to retaining terms up to fourth order in the fine-structure constant. The breakdown of the various contributions arising from the product in eq. 1 are summarised in Table I. The first group of terms named 'CONTACT' depends on the delocalization of unpaired-electron spin density to the nuclear position of the OC; the second 'DIPOLAR' group gathers terms that depend on the electron-nuclear magnetic dipolar interaction, and therefore on the spatial position of the unpaired electrons relative to the OC and the relative orientation of their magnetic moments.

Another useful distinction for the interpretation of $\boldsymbol{\sigma}^s$ in terms of the structural and electronic properties concerns the rank of the spherical tensors corresponding to the various terms in Table I. The rank-zero terms lead to an isotropic paramagnetic shift, whereas the rank-two terms represent a shift anisotropy. Rank-one terms do not give rise to observable features in the spectrum under high-field conditions, and so are not considered further. In particular, the non-relativistic Fermi contact shift corresponds to the element of the shielding tensor arising from the coupling in term (a) of Table I [14]. This constitutes the isotropic contribution that depends on the electronic structure of the TM and on the degree of covalency and the orbital overlap in the bond linking the OC and the TM. Term (a) is commonly the dominant isotropic contact contribution in systems where the delo-

TYPE	TERM	EXPRESSION	RANK
CONTACT	a)	$g_e A^{\mathrm{FC}}$	0
	b)	$g_e A^{\mathrm{FC},2}$	0
	c)	$\Delta g_{\mathrm{iso}} A^{\mathrm{FC}}$	0
	d)	$A^{\mathrm{FC}} \boldsymbol{\Delta\tilde{g}}$	1,2
DIPOLAR	e)	$g_e \boldsymbol{A}^{\mathrm{dip}}$	2
	f)	$g_e \boldsymbol{A}^{\mathrm{dip},2}$	2
	g)	$\Delta g_{\mathrm{iso}} \boldsymbol{A}^{\mathrm{dip}}$	2
	h)	$\boldsymbol{\Delta\tilde{g}} \boldsymbol{A}^{\mathrm{dip}}$	0,1,2

TABLE I. Comparison of the terms contributing to the paramagnetic shielding tensor in eq. 1 from the coupling between the hyperfine and g-tensors in eq. 2. The terms are gathered into two groups. The terms in the first group are due to an isotropic contact hyperfine interaction (CONTACT), and the second group contains terms due to an anisotropic electron-nuclear dipolar hyperfine interaction (DIPOLAR); for each product, the ranks of the resulting irreducible spherical tensor(s) contributions to the shielding are given.

calization of the unpaired-electron spin density from the TM sites towards the s orbitals of the OC is prominent [36]. Terms (b), (c) and (d) represent the spin-orbit coupling contributions to the total contact shielding, either *via* the g-shift or the spin-orbit-based $A^{\mathrm{FC},2}$ term. In particular, term (c) accounts for the spin-orbit deviation of the isotropic g-shift from the free-electron value, giving rise to a contribution proportional to A^{FC}. It will be shown later how this term turns out to contribute significantly to the total isotropic shift of the OC, in the systems studied in this work. In doublet systems, term (h) in Table I is commonly referred to as the pseudo-contact shift. It derives from the coupling between the non-relativistic dipolar component of the hyperfine tensor and the g-anisotropy due to spin-orbit coupling [15]. As the pseudo-contact term arises from the dipolar hyperfine interaction, it leads to a shift that depends on the spatial position and orientation of the magnetic moment of the unpaired-electron spin density relative to the nuclear magnetic moment of the OC. Considering the rank-two terms of Table I, these contribute to the spectrum in the form of the shift anisotropy. Term (e) of Table I represents the only non-relativistic dipolar contribution to the anisotropy, and it depends on the magnitude of the electronic and nuclear magnetic moments involved in the dipolar interaction, on their relative orientation and on their separation in space. All the other terms of the group - (f), (g) and the rank-two contribution of term (h) - account for the spin-orbit corrections to this dipolar anisotropy. The other relativistic contribution to the shift anisotropy comes from the rank-two term (d), which is due to the g-anisotropy and the isotropic Fermi contact component of the hyperfine interaction. For solids in which the TM ions are a major constituent of the lattice, the total paramagnetic shielding at the OC is the combination of the various contributions to the isotropic shift and shift anisotropy from all the TM sites. Solid-state density functional theory (DFT) calculations have been shown to be extremely helpful in unravelling the NMR response of paramagnetic solids containing multiple paramagnetic centres [13, 29, 37, 38]. The approach for the calculation of the Fermi contact shifts and shift anisotropy in paramagnetic solids [12] is here extended to include the spin-orbit coupling effect. In Ref. 12, the methodology for computing Fermi contact interactions in solids was developed in which, among other systems, the olivine-type $LiTMPO_4$ materials were used as model systems. In the following discussion of the treatment of spin-orbit coupling effects in solids the same systems are used to allow direct comparison with prior work.

A. Analysis of the g-tensor in solids

The unit cell of the olivine-type $LiTMPO_4$ structure with an orthorhombic *Pnma* space group is shown in Figure 1. In order to explore the relationship between the overall magnetic structure of the $LiTMPO_4$ unit cell and that of an individual magnetic centre, we now explore the symmetry relationships between the different TM sites. The four TM sites $\mathrm{I}-\mathrm{IV}$ occupy the same 4 c Wyckoff positions and have the following coordinates:

$$\begin{aligned} \mathrm{I} &: x+\frac{1}{2},\ \frac{1}{4},\ \bar{z}+\frac{1}{2} \\ \mathrm{II} &: \bar{x},\ \frac{3}{4},\ \bar{z} \\ \mathrm{III} &: \bar{x}+\frac{1}{2},\ \frac{3}{4},\ z+\frac{1}{2} \\ \mathrm{IV} &: x,\ \frac{1}{4},\ z \end{aligned} \tag{3}$$

These equivalent positions are related by symmetry operations as defined by the space group. For example, if we focus on the metal ion in site I, it transforms into site II *via* either a two-fold screw rotation with the axis parallel to c, or a diagonal glide reflection with the plane perpendicular to a; it transforms into III *via* either a rotoinversion or a two-fold screw rotation with the axis parallel to b and it transforms into IV *via* either a two-fold screw rotation with the axis parallel to a or an axial glide reflection with the plane perpendicular to c [39–41].

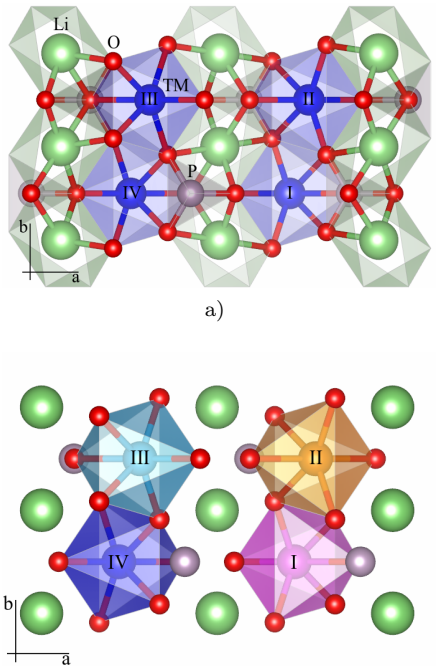

a)

b)

FIG. 1. (1a) Structure of the repeating unit of the olivine-type phase of $LiTMPO_4$ (TM=Mn, Fe, Co, Ni) consisting of a distorted hexagonal close-packed oxygen (red) framework. Phosphorus (pink) occupies an eighth of the tetrahedral sites, while the two octahedral sites are occupied by lithium (green) and the TM (blue). (1b) The four octahedral TM sites are labelled I, II, III, IV and occupy different spatial positions: their environments (in pink, orange, light blue and blue respectively) are related to one another as according to the orthorhombic symmetry of the *Pnma* space group.

All these relations are summarised in eq. 4:

$$\begin{aligned} &\mathrm{I} \leftrightarrow \mathrm{II} : 2(0,0,\frac{1}{2})\ \frac{1}{4},0,z\ ;\ n(0,\frac{1}{2},\frac{1}{2})\ \frac{1}{4},y,z \\ &\mathrm{I} \leftrightarrow \mathrm{III} : \bar{1}\ 0,0,0\ ;\ 2(0,\frac{1}{2},0)\ 0,y,0 \\ &\mathrm{I} \leftrightarrow \mathrm{IV} : 2(\frac{1}{2},0,0)\ x,\frac{1}{4},\frac{1}{4}\ ;\ a\ x,y,\frac{1}{4} \end{aligned} \tag{4}$$

In the case where the system contains a unique TM species in a particular electronic state in the weak exchange-coupling regime [42], the orientations of the site-specific g-tensors are related by the same operations defining the symmetry of the unit cell. In the *Pnma* space group discussed here, these are the same operations summarised in eq. 4 [43, 44]. Consider for instance the g-tensor of site I in Figure 1b and its relation with those of the other sites: because of the operations given above, when expressed with respect to the same reference frame, such as the unit-cell frame, the g-shift tensors of sites I – IV are found to be:

$$\boldsymbol{\Delta g}_{\mathrm{I}} = \begin{pmatrix} \Delta g_{\mathrm{I}}^{x,x} & \Delta g_{\mathrm{I}}^{x,y} & \Delta g_{\mathrm{I}}^{x,z} \\ \Delta g_{\mathrm{I}}^{y,x} & \Delta g_{\mathrm{I}}^{y,y} & \Delta g_{\mathrm{I}}^{y,z} \\ \Delta g_{\mathrm{I}}^{z,x} & \Delta g_{\mathrm{I}}^{z,y} & \Delta g_{\mathrm{I}}^{z,z} \end{pmatrix} \tag{5a}$$

$$\boldsymbol{\Delta g}_{\mathrm{II}} = \begin{pmatrix} \Delta g_{\mathrm{I}}^{x,x} & -\Delta g_{\mathrm{I}}^{x,y} & -\Delta g_{\mathrm{I}}^{x,z} \\ -\Delta g_{\mathrm{I}}^{y,x} & \Delta g_{\mathrm{I}}^{y,y} & \Delta g_{\mathrm{I}}^{y,z} \\ -\Delta g_{\mathrm{I}}^{z,x} & \Delta g_{\mathrm{I}}^{z,y} & \Delta g_{\mathrm{I}}^{z,z} \end{pmatrix} \tag{5b}$$

$$\boldsymbol{\Delta g}_{\mathrm{III}} = \begin{pmatrix} \Delta g_{\mathrm{I}}^{x,x} & -\Delta g_{\mathrm{I}}^{x,y} & \Delta g_{\mathrm{I}}^{x,z} \\ -\Delta g_{\mathrm{I}}^{y,x} & \Delta g_{\mathrm{I}}^{y,y} & -\Delta g_{\mathrm{I}}^{y,z} \\ \Delta g_{\mathrm{I}}^{z,x} & -\Delta g_{\mathrm{I}}^{z,y} & \Delta g_{\mathrm{I}}^{z,z} \end{pmatrix} \tag{5c}$$

$$\boldsymbol{\Delta g}_{\mathrm{IV}} = \begin{pmatrix} \Delta g_{\mathrm{I}}^{x,x} & \Delta g_{\mathrm{I}}^{x,y} & -\Delta g_{\mathrm{I}}^{x,z} \\ \Delta g_{\mathrm{I}}^{y,x} & \Delta g_{\mathrm{I}}^{y,y} & -\Delta g_{\mathrm{I}}^{y,z} \\ -\Delta g_{\mathrm{I}}^{z,x} & -\Delta g_{\mathrm{I}}^{z,y} & \Delta g_{\mathrm{I}}^{z,z} \end{pmatrix} \tag{5d}$$

As a result of the symmetry relations among the various TM environments in the orthorhombic group, the overall repeated-unit deviation from g_e results in a diagonal tensor, $\boldsymbol{\Delta g}_{\mathrm{r.u.}}$, being the sum of the Δg values of all the spin centres in the cell, with the form shown in eq. 6. Thus, the diagonal components of the per-site $\boldsymbol{\Delta g}$ are obtained by dividing the repeated-unit g-shift by the number of TM centres of the cell. It is important to stress that this result is not general and only occurs when all of the g-tensors of the individual transition metal centres are constrained to be collinear by the symmetry operations inherent to the space group symmetry of the lattice. We present a more general approach below that can be utilised under conditions where this is not the case.

$$\begin{aligned} \boldsymbol{\Delta g}_{\mathrm{r.u.}} &= \boldsymbol{\Delta g}_{\mathrm{I}} + \boldsymbol{\Delta g}_{\mathrm{II}} + \boldsymbol{\Delta g}_{\mathrm{III}} + \boldsymbol{\Delta g}_{\mathrm{IV}} \\ &= \begin{pmatrix} 4\ \Delta g_{\mathrm{I}}^{x,x} & 0 & 0 \\ 0 & 4\ \Delta g_{\mathrm{I}}^{y,y} & 0 \\ 0 & 0 & 4\ \Delta g_{\mathrm{I}}^{z,z} \end{pmatrix} \end{aligned} \tag{6}$$

B. Analysis of the hyperfine tensor in solids

The hyperfine tensor determining the paramagnetic shift of a particular observed site modulates the contact and dipolar interactions between the nuclear spin of the OC and the total spin of the unpaired electrons. In a system such as the above example where the weakly exchange-coupled TM ions are a major constituent of the lattice, the hyperfine tensor defined at the OC nuclear position is equal to the sum of the contact and dipolar interactions with each of the surrounding TM sites. It has been shown that the total Fermi contact term, A^{FC}, can be decomposed into the sum of all relevant pairwise TM-O-OC *bond-pathway* contributions, allowing the unpaired-electron spin density transferred for each individual TM site to the nuclear position of the OC to be computed [12]. For the dipolar component of the hyperfine tensor, the long-range anisotropic electron-nuclear interaction depends on the position vector originating at the OC which connects it to the unpaired-electron spin density of each TM site. For the olivine structure (Figure 2) the dipolar interaction between an OC, such as Li A, and a particular paramagnetic site, such as TM-I, is different to the interaction between Li A and TM-II because of their respective orientation. Also, the strength of the

dipolar interaction weakens with the distance between the involved centres, r, as $1/r^3$ [45].

C. Treatment of the Paramagnetic Shielding in Solids *via* DFT

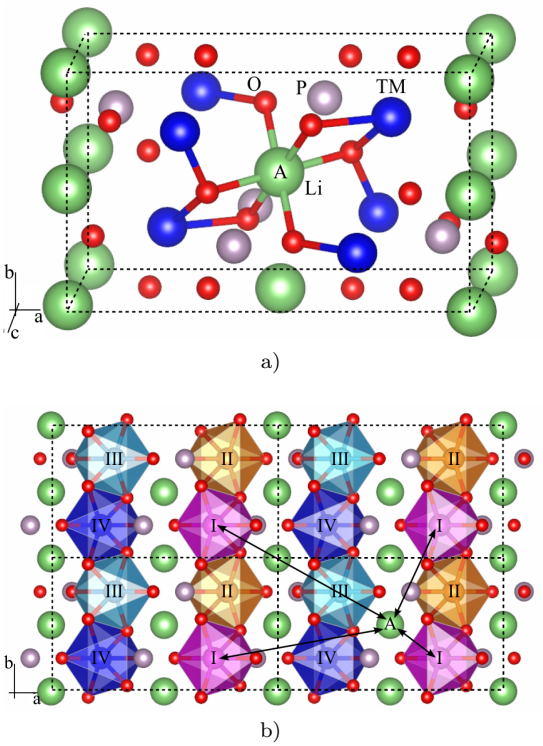

FIG. 2. (2a) Repeating unit of the olivine-type $LiTMPO_4$ delimited by the dashed box. The solid lines represent the pair-wise TM-O-Li bonds and denote the pathways of delocalization of unpaired-electron spin density from each TM site to the nuclear position of the OC, here the lithium site labelled A, as in Ref. 12. (2b) Periodic expansion of the $LiTMPO_4$ repeating unit; the arrows highlight the TM-OC pairs interacting *via* magnetic dipolar coupling, and specifically underline the interactions between the lithium site labelled A and one of the four inequivalent TM sites, here labelled as I, throughout the periodically repeating units.

A detailed insight into the NMR response in solids containing multiple paramagnetic centres is obtainable directly *via* periodic solid-state DFT studies. Previous works described how the *bond-pathway* decomposition of the isotropic Fermi contact component of the total hyperfine tensor can be calculated with DFT *via* the so-called *spin-flipping* approach [12]. In this method, the total Fermi contact term is calculated from the spin density at the OC nuclear position in a ferromagnetic state. The individual shift contribution of a TM-O-OC pathway is then calculated by flipping the spin of the TM ion in the repeated unit. The difference in the spin density between the ferromagnetic and the flipped states gives the Fermi contact contribution of the corresponding pathway. In general the approach proves particularly accurate [12] because the unpaired-electron delocalization is a short-range interaction. In the present study, we demonstrate how the total dipolar hyperfine coupling can be decomposed using a similar method. Firstly, the total dipolar hyperfine tensor is calculated at the OC as a result of its magnetic interactions with all the TM sites in the ferromagnetic state. Subsequently, the TM-specific contributions to the total dipolar term are obtained separately by flipping each of the four TM spins labelled $\mathrm{I}-\mathrm{IV}$ in the cell in Figure 2b. The difference in the OC dipolar tensor due to the flip gives the contribution from each TM site. As shown in Figure 2b for TM-I, flipping the spin of a paramagnetic centre in the unit cell results in the spins of the same site in *all* neighbouring cells being flipped. The resulting contribution to the dipolar tensor calculated at a particular OC, such as Li A in Figure 2b, is then due to the interaction of its nuclear moment with the electronic moment of *all* the TM I ions throughout the lattice. This approach ensures that the spatial and orientational dependence of the coupling are properly treated *via* the periodic boundary conditions (PBC). The additivity of the contributions can be assessed by comparison with the ferromagnetic alignment of all the TM spins, as for the Fermi contact analysis [12].

In the current DFT approach, the g-tensor for a material containing multiple paramagnetic centres is calculated by linear response [46, 47], which results in a single overall g-tensor for the cell. The contribution to the g-tensor from a particular TM site can be calculated by replacing the other TM sites in the cell with diamagnetic atoms. Care must be taken in order to make sure that the resulting local distortions are negligible and that the repeated unit is expanded enough so to avoid long-range interactions between TM sites through the PBC. Using this procedure, the only source of spin-orbit coupling is due to the remaining paramagnetic centre and hence we obtain the g-tensor of this ion. By calculating the $\boldsymbol{\Delta g}$ for each TM site, the off-diagonal components of the g-tensor are computed, which are required to give an accurate description of the coupling with the $\boldsymbol{A}^{\mathrm{dip}}$ tensor. Once the $\boldsymbol{g}$ and $\boldsymbol{A}^{\mathrm{dip}}$ tensors have been computed, they are combined to give the shielding tensor in eq. 1. As a result of the limitations of the available computational methods for solid-state DFT, to the best of our knowledge the calculation of the hyperfine relativistic corrections ($A^{\mathrm{FC},2}, \boldsymbol{A}^{\mathrm{dip},2}$) are not currently possible, and so we do not comment further on terms (b) and (f) of Table I, which are expected to be small for ligand hyperfine couplings, except for nuclei directly bonded to truly heavy centres [48, 49]. The overall isotropic paramagnetic shift for an OC is calculated as the sum of the contact terms (a) and (c) and the rank-zero component of term (h). For the former two terms, we calculate the total A^{FC} in the ferromagnetic state and the sum of the four TM-specific

Δg_{iso} separately; for the latter we calculate separately the coupling between the $\boldsymbol{\Delta g}$ of each of the four TM sites and the corresponding $\boldsymbol{A}^{\text{dip}}$ tensor isolated *via* the aforementioned *spin-flip* approach. To obtain the total shielding tensor, we sum the various products of these contributions and extract the corresponding isotropic, anisotropic and asymmetry values.

III. COMPUTATIONAL METHODS

First-principles solid-state DFT calculations were performed within the Linear Combination of Atomic Orbital (LCAO) scheme with the CRYSTAL09 Code [50, 51] and the Generalized Gradient Approximation (GGA) scheme with the QuantumEspresso Package [52]. The calculation of the hyperfine properties was performed in CRYSTAL09 as previous studies [12, 53] have shown that the use of hybrid functionals in an all-electron treatment provides good agreement with experiments. For this, three hybrid exchange-correlation functionals were used: the PBE0 incorporating 25% Hartree-Fock (HF) exchange [54, 55], shown to provide satisfactory performances for the electronic and magnetic structures of the class of materials of interest [53], and the related 20% HF hybrid (PBE20) and 35% HF hybrid (PBE35). The choice of studying these systems with a range of hybrid functionals was motivated by the known sensitivity of the electronic delocalisation and spin polarisation on the percent of HF exchange included [12, 53, 56, 57]. Two levels of all-electron atom-centered basis set were used, a smaller set used for structure optimisation and a more extended one used for hyperfine calculations [12]. A total energy tolerance of 10^{-7} a.u. was chosen and the reciprocal-space sampling was performed with k-point grids of $2 \times 3 \times 4$ points in the $LiTMPO_4$ unit cell. Full details of the computational method are reported in the S.I.

As spin-orbit coupling effects are not treated in the version of CRYSTAL used in this study, the Projector Augmented Wave (PAW) [58] QuantumEspresso package was used to calculate g-tensors for the same systems, supported by previously presented results obtained within this scheme [30]. For these calculations, the PBE exchange functional was chosen [54]. Scalar-relativistic norm-conserving pseudopotentials with nonlinear core correction were used, and the all-electron information was reconstructed using PAW and gauge-including projector augmented-wave (GIPAW) [46, 47]. A plane wave cutoff energy of 900 eV was chosen, yielding an energy convergence to within 6 meV per atom. The same energy tolerance and k-mesh sampling as used in the CRYSTAL calculations were once again used. For the calculation of per-site g-tensors, a $1 \times 2 \times 2$ supercell expansion of the crystallographic primitive cell was required, associated with a k-sampling of $2 \times 2 \times 2$. These supercells were made almost entirely diamagnetic by substituting all but the TM site under study with Mg^{2+} ions. In the GIPAW implementation in the Quantum-Espresso package, a mean-field approximation to the many-body Hamiltonian is made and as a result, the spin-orbit and spin-other-orbit operators are represented as a sum of one-electron terms, according to Ref. 47. Hybrid functionals were not used as the calculation of the g-tensor *via* the linear response method is not currently supported with these. Hence, calculations of g-tensors were compared for a pure GGA method and a GGA+U method with the PBE functional. As will be discussed below, the former is more appropriate for g-tensor calculations. The latter method, which is widely used in periodic DFT calculations of transition metal-contain systems, is an alternative approach to the hybrid treatment and it involves the addition of a Hubbard U correction [59] to specific subshells - here the $3d$ TM orbitals - to correct for effects due to the incorrect treatment of electron correlations with the DFT approach [60]. This has previously been shown to improve the description of the magnetic coupling constants and the electronic structure of transition metal oxide systems [61–64], and to accurately predict the respective ground-state d-level splitting pattern [65]. The rotationally invariant treatment of U proposed by Dudarev *et al.* was here used [66], in which a single U_{eff} parameter is applied to the d electrons of the transition metal species. The values of U_{eff} were chosen from previous self-consistent determinations [61] and are reported in Table II. The effect and validity of the addition of U to g-tensor calculations is explored.

The structures of $LiMnPO_4$ [67], $LiFePO_4$ [68] and $LiNiPO_4$ [67] were fully relaxed with both DFT packages independently. For $LiCoPO_4$, the experimental structure (Ref. 69) was used without further relaxation in order to avoid the difficulties in optimising the distinct sublattice anions, as described in detail by Middlemiss *et al.* [12]. Furthermore, as derived in Ref. 29, the bulk magnetic properties of the materials affect the paramagnetic shift. These effects are included in the treatment by modifying the temperature dependence of the shift *via* the inclusion of the Weiss constant Θ. Hence, the prefactor in eq. 1 used to calculate all terms in the $\boldsymbol{\sigma^s}$ becomes $-\frac{\mu_B S(S+1)}{3\hbar\gamma_N K_B (T-\Theta)}$. The temperature used in this work was 320 K to approximate the frictional heating due to Magic Angle Spinning (MAS). The Weiss constants used for $LiMnPO_4$, $LiFePO_4$, $LiCoPO_4$ and $LiNiPO_4$ are summarised in Table II [33]. For all of the materials considered, the magnitude of the Weiss constant was found to be much lower than the experimental temperature $T = 320\ K$, which suggests that the spins can be treated as being essentially uncoupled from each other as a result of thermal fluctuations. For every calculated tensor, λ, the resulting isotropic term λ_{iso}, symmetric anisotropic value $\Delta\lambda$ and asymmetry parameter η were calculated following the convention in Ref. 70. For any symmetric tensor in the principal axis frame, the diagonal components are ordered such that $|\lambda_{zz} - \lambda_{\text{iso}}| > |\lambda_{yy} - \lambda_{\text{iso}}| > |\lambda_{xx} - \lambda_{\text{iso}}|$, with λ_{iso} being

the isotropic value defined in eq. 7, together with the second-rank tensor anisotropy, $\Delta\lambda$, and the asymmetry parameter, η:

$$\begin{aligned} \lambda_{\text{iso}} &= \frac{\lambda_{xx} + \lambda_{yy} + \lambda_{zz}}{3} \\ \Delta\lambda &= \lambda_{zz} - \lambda_{\text{iso}} \\ \eta &= \frac{\lambda_{xx} - \lambda_{yy}}{\Delta\lambda} \end{aligned} \tag{7}$$

For the systems studied in this work, no explicit calculation of the orbital component of the shielding tensor was included [17], as this contribution is very close to 0 ppm for the diamagnetic analogue material $LiMgPO_4$ [71].

Phosphate	S	$\mu_{\text{eff}}^{\text{theo}}$ [a] [μ_B]	$\mu_{\text{eff}}^{\text{expt}}$ [a] [μ_B]	Θ [a] [K]	U_{eff} [b] [eV]
$LiMnPO_4$	2.5	5.91	5.4	-58	3.92
$LiFePO_4$	2	4.89	6.8	-161	3.71
$LiCoPO_4$	1.5	3.87	5.0	-77	5.05
$LiNiPO_4$	1	2.82	3.1	-60	5.26

TABLE II. Summary of the parameters used in the calculation of hyperfine shifts: S, the spin quantum number of the TM ion involved in each phosphate; the theoretical ($\mu_{\text{eff}}^{\text{theo}}$) and experimental ($\mu_{\text{eff}}^{\text{expt}}$) magnetic moments in terms of the Bohr magneton (μ_B); Θ, the Weiss constant in Kelvin; U_{eff}, the effective Hubbard correction applied to the relative TM ion in eV. [a] Ref. 33. [b] Ref. 61.

IV. RESULTS AND DISCUSSION

For all the olivine $LiTMPO_4$ structures considered in this work, the experimentally observed unit cell parameters were in reasonable agreement with the optimised unit cell parameters obtained from hybrid functionals (LCAO), GGA and GGA+U approaches, as shown in Table S1 of the S.I. The results of the g-tensor calculations are also shown in detail in the S.I. As discussed in Section II for systems of orthorhombic symmetry, for all the studied phosphates the spin-orbit coupling effects at each TM site of the repeated unit are found to lead to g-tensors with the same principal components, which are oriented relative to each other according to the symmetry operations of the cell (eq. 5). The site-specific g-tensors and the values obtained for the whole repeated unit comprising all paramagnetic ions are compared in the S.I., the sum of the per-site g-tensors being very close to the *repeated unit* $\boldsymbol{g}_{\text{u.c.}}$ as expected from eq. 6. Table III shows the isotropic g_{iso} values calculated for an individual TM site for the four studied

TM	TM conf.	$\tilde{g}_{aa}$, $\tilde{g}_{bb}$, $\tilde{g}_{cc}$		g_{iso}		$g_{\text{iso}}^{\text{expt}}$
		GGA	GGA+U	GGA	GGA+U	
Mn^{2+}	$t_{2g}^3\ e_g^{*2}$	2.00	2.00	2.00	2.00	2.00 [a]
Fe^{2+}	$t_{2g}^4\ e_g^{*2}$	2.17, 2.23, 2.10	2.06, 2.03, 2.11	2.17	2.07	2.02 – 2.22 [b]
Co^{2+}	$t_{2g}^5\ e_g^{*2}$	2.26, 2.40, 2.39	2.16, 2.12, 2.12	2.35	2.13	2.17 – 2.36 [c]
Ni^{2+}	$t_{2g}^6\ e_g^{*2}$	2.25, 2.23, 2.25	2.14, 2.14, 2.13	2.24	2.14	2.15 [d]

TABLE III. Comparison of the electronic configuration and the calculated g-tensors for each different TM site in an octahedral crystal field as involved in the studied systems. For each ion, the occupation of the $3d$ orbitals in an octahedral field is specified. For each calculated TM-specific g-tensor the corresponding principal components ($\tilde{g}_{aa}$, $\tilde{g}_{bb}$, $\tilde{g}_{cc}$) and isotropic value (g_{iso}), calculated with pure GGA and with GGA+U, are reported and compared with theisotropic g value determined experimentally with EPR ($g_{\text{iso}}^{\text{expt}}$). [a] Ref. 72, 73. [b] Ref. 74, 75. [c] Ref. 74, 76, 77. [d] Ref. 78.

phosphates. Firstly it is clear from Table III that the range of experimentally-determined isotropic g values obtained from electron paramagnetic resonance (EPR) is broad for this class of $LiTMPO_4$ olivine systems, justifying further calculations to extract this parameter. All the calculated values of g_{iso} show a positive deviation from the free-electron g-value as expected for TM ions with a more-than-half-filled $3d$ shell. The results reflect the trends expected based on the electronic structure of the involved ions [45, 79]. The deviation from g_e is found to be negligible for Mn^{2+} as it has zero spin-orbit coupling as a result of the half-filled $3d$ shell. For Fe^{2+}, the effects of spin-orbit coupling result in a small deviation from g_e, with a calculated isotropic g-shift that falls within the experimental values shown in Table III. The effect of the spin-orbit coupling increases for octahedral Co^{2+}, largely due to the increased value of the spin-orbit coupling parameter moving across the 3d series, which results in a larger deviation from g_e.

The dependence of Δg_{iso} on the applied U_{eff} was studied, and the results are shown in Figure 3. In all cases the deviation from the free-electron g-value is found to decrease with increasing U_{eff} (converging to a plateau at high U_{eff} [80]). This is at first sight surprising, as it is known that the Fermi contact shift for the same systems [81] decreases with increasing U_{eff}, due to a reduction of the spin delocalisation from the $3d$ orbitals to the nucleus of interest - which, in the study in Ref. 81, is Li. One would expect the resulting larger spin density at the metal centre to enhance the g-tensor, due to larger spin-orbit contributions from the heavier centre. This is what one observes in g-tensor calculations on molecular $3d$-complexes, where adding more exact exchange to a hybrid functional increases the g-tensors [57]. Then why do Hubbard $+U$ corrections provide a change in the opposite direction? The reason is the increased energy gap,

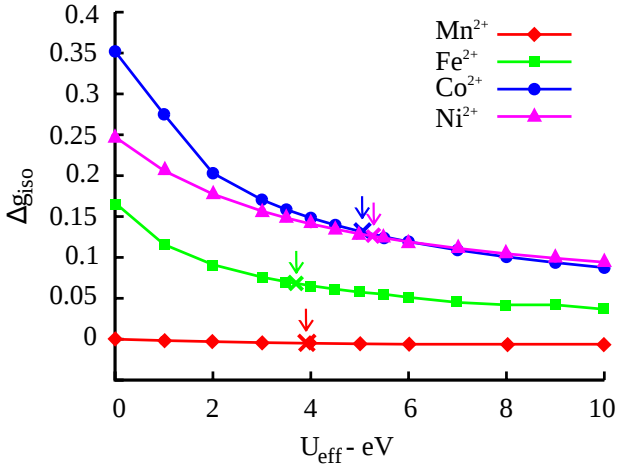

FIG. 3. Calculated isotropic value of the g-tensor shift, $\Delta g_{\rm iso}$, as a function of the $U_{\rm eff}$ correction applied on Mn^{2+} (in red prisms), Fe^{2+} (in green squares), Co^{2+} (in blue circles) and Ni^{2+} (in magenta triangles). For each case the isotropic value obtained with the $U_{\rm eff}$ value used in prior DFT+U studies is indicated with a cross.

which weakens the spin-orbit response contributions to the g-tensor (the gap enters the energy denominator of the perturbation expressions). While the same increase of the gap also occurs with increasing HF exchange in hybrid functionals, in the latter case the effect is overcompensated by the enhanced coupling terms contributed by the non-local HF exchange potential [57], leading to an overall increased linear response. Such coupling terms are absent in the DFT+U scheme, and thus the Hubbard terms move the results in the wrong direction. While comparison with experimental $\Delta g_{\rm iso}$ (Table III) might suggest improved agreement for DFT+U, this would indeed be due to compensation with other errors. We thus have to conclude that, while DFT+U improves hyperfine interactions, magnetic moments, band gap, and other aspects of electronic structure in the present $LiTMPO_4$ systems [63, 82–86], it is not suitable for response properties, unless one finds a way to mimic the response coupling terms. A correct treatment of solid-state g-tensors with hybrid functionals may provide a better route for future improvement. Here we will pragmatically use the uncorrected GGA results for the g-tensors and will combine them with hybrid-functional data for the hyperfine tensors. The results obtained within the GGA+U scheme are reported in the S.I. for completeness.

The paramagnetic shielding tensor is calculated by combining the g-tensor data with the hyperfine results according to eq. 1. The breakdown of the contributing terms presented in Table I is shown for the studied systems in Table IV. The hyperfine parameters are sensitive to the amount of Hartree-Fock exchange in the hybrid functional, as smaller amounts of HF exchange lead to more delocalization of the d orbitals. For simplicity, in Table IV we only show the PBE0 results, while the PBE20 and PBE35 results, which can be considered as upper and lower bounds of the acceptable range [12, 53], are shown in Tables 2-5 of the S.I. We now draw attention to the contributions to the isotropic shift resulting from the non-relativistic - term (a) - and relativistic - terms (c) and (h). With regards to the Fermi contact shift (a), the value of the isotropic term depends on the fraction of unpaired-electron spin density transferred from the d orbitals of the TM onto the s orbitals of the OC and on the covalency of the TM-O-OC bonds. From the ^{31}P results, the Fermi contact shift is found to decrease across the series going from Mn^{2+} towards Ni^{2+}, in line with the decrease of the number of unpaired electrons in the t_{2g} orbitals of the d-shell of the respective ions. Different unpaired-electron spin density transfer mechanisms are involved in the different bond-pathway configurations, as elucidated by Carlier *et al.* [13] for oxide based systems. This can be seen by comparing the values of term (a) in Table IV for ^7Li: after the decrease of the Fermi contact shift from the Mn^{2+} to Fe^{2+}, caused by the smaller number of unpaired t_{2g} electrons, we see that the sign of the shift, and hence of the transferred spin density, inverts on going from Fe^{2+} to Co^{2+} and Ni^{2+}. For the Fe site, there is an equal contribution of spin density transferred *via* a 90° pathway from the unpaired electrons in t_{2g} orbitals and a 180° pathway from the unpaired electrons in e_g orbitals towards the Li site. In the first case this corresponds to a positive transfer *via* a delocalization mechanism while in the second case, this leads to a negative transfer *via* a polarization mechanism. Hence the overall ^7Li Fermi contact shift in $LiFePO_4$ is the result of these opposite contributions. For the high-spin Co^{2+} case, the majority of spin density is transferred from e_g orbitals and the overall sign of the resulting Fermi contact shift becomes negative; finally for the Ni^{2+} case all the spin density is transferred from the e_g orbitals of the TM, leading to a larger and still negative shift. Regarding the term (c) in Table IV, this contribution to the isotropic shift represents the spin-orbit coupling correction to the Fermi contact interaction *via* the isotropic g-shift. By comparing the results for the different cases, this term scales with the extent of spin-orbit coupling for the involved TM ion. Term (c) for ^7Li is negligible for the Mn^{2+} case (0.3 ppm) and becomes progressively more significant when going from Fe^{2+} (9.0 ppm) to Ni^{2+} (-31.4 ppm). This term depends on the strength of the Fermi contact interaction, and it is interestingly shown to be non-negligible, particularly for the ^{31}P shift, due to the magnitude of $A^{\rm FC}$ for this nucleus.

We focus now on the isotropic term resulting from the product (h) in Table IV corresponding to the aforementioned pseudo-contact shift. We notice how the combination of spin-orbit coupling and dipolar interaction results in a non obvious trend for this isotropic shift. Although the deviation from the g-value almost doubles in going from Fe^{2+} to Co^{2+}, the dipolar interaction is reduced to the point where the magnitude of the overall pseudo-contact shift is larger for the former than for the latter. This result suggests that although the ^7Li shift is dom-

		CONTACT TERMS									DIPOLAR TERMS									ISOTROPIC TERM	
		a) $g_e A^{FC}$			c) $\Delta g_{iso} A^{FC}$			d) $A^{FC}\Delta\tilde{g}$			e) $g_e \boldsymbol{A}^{dip}$			g) $\Delta g_{iso} \boldsymbol{A}^{dip}$			h) $\Delta\tilde{g}\boldsymbol{A}^{dip}$			DFT	EXP
		δ_{iso} [ppm]	$\Delta\delta$ [ppm]	η	δ_{iso} [ppm]	$\Delta\delta$ [ppm]	η	δ_{iso} [ppm]	$\Delta\delta$ [ppm]	η	δ_{iso} [ppm]	$\Delta\delta$ [ppm]	η	δ_{iso} [ppm]	$\Delta\delta$ [ppm]	η	δ_{iso} [ppm]	$\Delta\delta$ [ppm]	η	δ_{iso} [ppm]	δ_{iso} [ppm]
^{7}Li	$LiMnPO_4$	109.9	0	—	0.3	0	—	0	0.1	0.3	0	1234.2	0.2	0	0.9	0.2	-0.1	0.2	0.4	110.1	57[a], 68[b]
	$LiFePO_4$	27.2	0	—	9.0	0	—	0	-3.6	0.9	0	881.0	0.2	0	72.7	0.2	-1.2	-15.3	0.7	35.0	-15[a], -8[b]
	$LiCoPO_4$	-19.6	0	—	-13.5	0	—	0	3.6	0.1	0	700.3	0.2	0	121.0	0.2	-17.8	-14.5	0.4	-50.9	-92[a], -86[b]
	$LiNiPO_4$	-64.8	0	—	-31.4	0	—	0	2.0	0.1	0	433.8	0.2	0	52.6	0.2	-0.9	-1.6	0.3	-97.1	-49[b], -41[a]
^{31}P	$LiMnPO_4$	8397.3	0	—	25.3	0	—	0	11.3	0.3	0	795.9	0.5	0	-1.2	0.5	-0.1	0.2	0.3	8404.5	7296[a]
	$LiFePO_4$	3219.0	0	—	1062.9	0	—	0	-432.2	0.96	0	795.4	0.4	0	65.7	0.4	-2.4	13.4	0.2	4279.5	3352[a]
	$LiCoPO_4$	2012.6	0	—	1391.5	0	—	0	-369.3	0.1	0	652.6	0.4	0	112.8	0.4	-3.8	9.2	0.6	3400.3	2756[a]
	$LiNiPO_4$	1658.7	0	—	804.3	0	—	0	-50.4	0.4	0	576.1	0.1	0	69.9	0.1	1.1	-2.2	0.1	2462.1	1706[a]

TABLE IV. Comparison of the various terms contributing to the shielding tensor for the series of $LiTMPO_4$ compounds (TM= Mn, Fe, Co, Ni) at the ^{7}Li and ^{31}P sites broken down into the contact and dipolar isotropic shift (δ_{iso}, ppm), symmetric anisotropic value ($\Delta\delta$, ppm) and asymmetry parameter (η, dimensionless). The hyperfine tensor for this Table is obtained with the PBE0 hybrid functional and the g-tensor is calculated at PBE GGA level. Every tensorial term of the Table is reported oriented with respect to its own principal axis frame. All the reported terms are scaled by the pre-factor $-\frac{\mu_B S(S+1)}{3\hbar\gamma_N K_B(T-\Theta)}$, with the respective Weiss constant of the system reported in Table II. The last column compares the sum of the calculated isotropic terms (a, c, h) with the experimental isotropic shift. [a] Ref. [34]. [b] Ref. [33].

	^{7}Li				^{31}P			
	δ_{iso} [a] [ppm]	$\Delta\delta^{DFT}$ [ppm]	$\Delta\delta^{FIT}$ [ppm]	η^{FIT}	δ_{iso} [a] [ppm]	$\Delta\delta^{DFT}$ [ppm]	$\Delta\delta^{FIT}$ [ppm]	η^{FIT}
$LiMnPO_4$	67.9	1241.3	1159.9	0.8	7879	1098.9	963.3	0.8
$LiFePO_4$	-16.8	884.6	1115.1	0.7	3558	-830.6	-865.0	0.7

TABLE V. Results of the DFT calculated and fitted shielding anisotropy for ^{7}Li and ^{31}P spectra of $LiMnPO_4$ (shown in Figure 4a and 4c respectively) and of $LiFePO_4$ (shown in Figure 4b and 4d respectively). The results are reported as the isotropic shift (δ_{iso}, ppm), the symmetric anisotropic value ($\Delta\delta$, ppm) and the asymmetry parameter (η, dimensionless). [a] The experimental spectra as well as the reported values for the isotropic shifts (δ_{iso}) are taken from Ref. 37.

inated by the contact contribution, the pseudo-contact term can be non-negligible in these systems. The agreement between the total isotropic shift obtained with DFT and the experimental value is still not particularly good for the ^{7}Li site. Part of the discrepancy is thought to be due to the neglect of the zero-field splitting effects. Also, a careful analysis of the basis set and of structural optimization is under investigation by some of the authors of this work, which are expected to have an effect on the accuracy of the spin-density calculated at the nuclear position. For ^{31}P the agreement is more satisfactory, mainly because of the predominance of the Fermi contact contribution to the total shift, as previously described. We now discuss the terms in Table IV contributing to the shift anisotropy, both non-relativistic (e) and due to spin-orbit coupling ((d), (g), (h)). Focusing on the dipolar component of the hyperfine tensor, $\boldsymbol{A}^{dip}$, there is a decrease along the series from Mn to Ni, hence giving a progressively smaller contribution to the shift anisotropy, as seen by comparing terms (e) of Table IV. The calculated tensor with no spin-orbit coupling inclusion corresponds to the dipolar interaction between the magnetic moments of the observed nucleus and magnetic moment of the TM ion [29, 36]. Following the trend of μ_{eff}^{theo} for

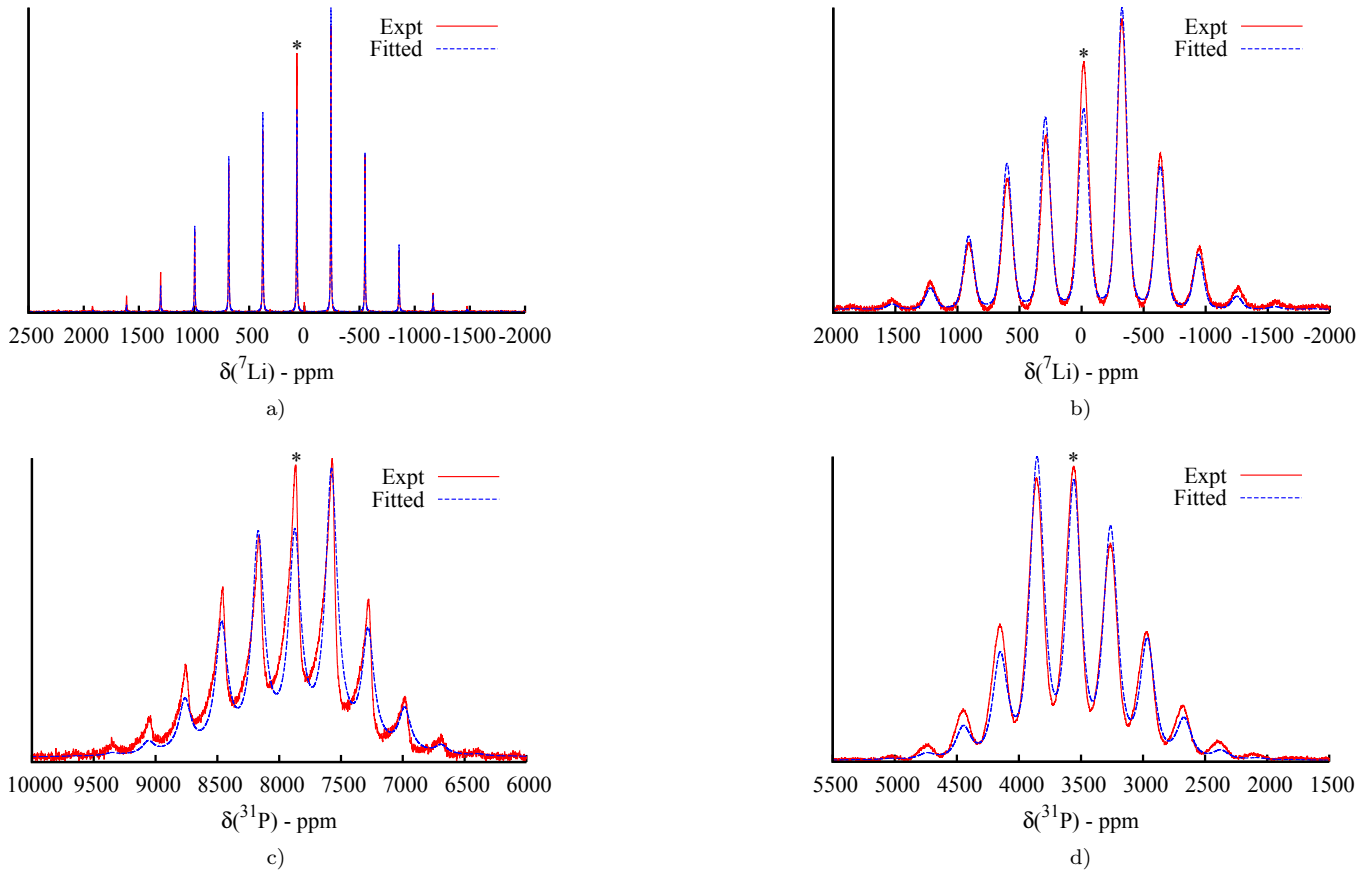

FIG. 4. Experimental (in solid red line) and fitted (in dashed blue line) ^{7}Li and ^{31}P spectra of $LiMnPO_4$ (Figure 4a and 4c respectively) and $LiFePO_4$ (Figure 4b and 4d respectively). Isotropic peaks are marked with an asterisk. The experimental spectra are taken from Ref. 37.

the considered ions reported in Table II, a progressively weaker dipolar interaction is observed when going from Mn^{2+} towards Ni^{2+}. The trend is more complex when spin-orbit coupling is included, as seen from Tables II and III: the $\boldsymbol{\Delta}g$ and $\boldsymbol{A}^{\mathrm{dip}}$ tensors involved in terms (g) and (h) of Table IV follow opposite trends along the series of studied systems. The contributions to the shift anisotropy are the product of these two terms, resulting in an increase in the anisotropy when going from Mn^{2+} to Fe^{2+} and a decrease when going from Fe^{2+} to Ni^{2+}. For ^{31}P the relativistic corrections to the shift anisotropy are found to contribute significantly to the total value. For $LiMnPO_4$ and $LiFePO_4$, the total shift anisotropy $\Delta\delta^{\mathrm{DFT}}$ is calculated from the coupling of the full $\boldsymbol{A}$ and $\boldsymbol{g}$ tensors as in eq. 1. We stress that these values cannot be obtained by directly summing the relevant terms - terms (d), (e), (g) and (h) in Table IV - since each of these terms is expressed with respect to its own principal frame, which is not necessarily unique for all the tensorial products. Thus, the direct sum of the reported $\Delta\delta$ values is not necessarily appropriate because of the different reference frames of the various terms. By coupling the whole hyperfine tensor and g-tensor we then obtain for ^{7}Li $\Delta\delta^{\mathrm{DFT}}(\mathrm{Mn}) = 1241.3$ ppm and $\Delta\delta^{\mathrm{DFT}}(\mathrm{Fe}) = 884.6$ ppm, while for the ^{31}P, $\Delta\delta^{\mathrm{DFT}}(\mathrm{Mn}) = 1098.9$ ppm and $\Delta\delta^{\mathrm{DFT}}(\mathrm{Fe}) = -830.6$ ppm. These values can be compared with the values of spin-dipolar anisotropy obtained by fitting the solid-state MAS ^{7}Li and ^{31}P NMR spectra of the $LiMnPO_4$ and $LiFePO_4$ powders (previously reported and shown in Figure S1 and Figure 1 of Ref. 37 for ^{7}Li and ^{31}P respectively). The results of the fitting carried out within the DMFIT software [87] are shown in Figure 4 and summarised in Table V. We point out that the values for the ^{7}Li and ^{31}P isotropic shifts measured in Ref. 34 and in Ref. 37, and reported in this work in Tables IV and V respectively, are not exactly equal. The NMR spectra of the two studies were acquired at different MAS speeds - 22.5 KHz in Ref. 34 and 60 KHz in Ref. 37. Hence, the discrepancy between the measured isotropic shifts is thought to be mainly due to the different temperatures experienced by the powder sample during the acquisition due to frictional heating caused by MAS. It is interesting to note that the DFT results predict, for the ^{7}Li spectra, a sideband pattern

of comparable width and anisotropy for both $LiMnPO_4$ and $LiFePO_4$, while for the ^{31}P spectra of the two phosphates the patterns are calculated to be of comparable width but of opposite anisotropy. These results are in reasonable agreement with the fitting of the experimental NMR spectra, as summarised in Table V. Of note, without the inclusion of spin-orbit coupling we would not have been able to reproduce the correct sign of the anisotropy for the ^{31}P shift of $LiFePO_4$. Errors between the fits and the observed spectra are largely caused by bulk magnetic susceptibility (BMS) effects, which vary from particle to particle and within a particle; BMS effects also contribute to the discrepancy between the calculations and the fits [88]. Despite our neglect of this term, this work represents to the best of our knowledge the first example of a paramagnetic NMR anisotropy pattern simulation where hyperfine and spin-orbit coupling parameters are obtained from first principles.

V. CONCLUSIONS

We have presented a method to include spin-orbit coupling effects in the calculation of the paramagnetic NMR shielding for solid systems with multiple paramagnetic centres. We demonstrate how to combine the Fermi contact and dipolar hyperfine interactions between the NMR-observed nucleus and multiple TM sites, with the g-tensor. The hyperfine interactions and g-tensors in this study are calculated from first principles through the use of solid-state DFT calculations. An accurate description of spin-orbit coupling effects on the NMR signal of such systems can only be obtained by including the g-tensor associated with each individual paramagnetic site of the solid. A calculation performed for a system containing multiple paramagnetic ions leads to an overall g-tensor for the whole unit cell. If the system contains paramagnetic ions with principal components along different directions (as dictated by the symmetry operations of the crystallographic space group of the material), or different types of paramagnetic ions, then the overall tensor is not a simple sum of the individual tensors of the different ions, unless they are all expressed with respect to a common reference frame. Furthermore, the overall computed tensor cannot be used to determine the tensors for the individual ions. Since the NMR and EPR parameters are influenced by the g-tensor of the individual ions, we adopted a simple approach to extract these parameters, which involved substituting all but one ion within the cell by diamagnetic ions. The first-principles approach is used to study the NMR response of a series of olivine $LiTMPO_4$ materials (TM=Mn, Fe, Co, Ni). In particular, we show the importance of including spin-orbit coupling effects in combination with the hyperfine interaction in order to obtain an accurate description of the observed NMR chemical shift and shift anisotropy. The approach outlined here can be readily applied to aid in the interpretation of the NMR spectra of a wide range of solid systems with multiple (and different) paramagnetic centres, allowing more detailed structural and electronic information to be extracted from these systems.

ACKNOWLEDGEMENT

All the authors are thankful to Prof. Chris J. Pickard, Dr. Derek S. Middlemiss, Dr. Ladislav Benda, Ms Raphaële J. Clément and Mr Arobendo Mondal for very useful discussions. RP acknowledges financial support from the People Programme (Marie Curie Actions) of the European Union's Seventh Framework Programme (FP7/2007-2013) under REA grant agreement n°317127. Via our membership of the U.K.'s HPC Materials Chemistry Consortium, which is funded by EPSRC (n°EP/L000202), this work made use of the facilities of ARCHER, the U.K.'s national high-performance computing service, which is funded by the Office of Science and Technology through EPSRC's High End Computing Programme. Research was also carried out at the Center for Functional Nanomaterials, Brookhaven National Laboratory, which is supported by the U.S. Department of Energy, Office of Basic Energy Sciences, under Contract n°DE-AC02-98CH10886.

[1] J. Finkelstein, Nature **460**, 813 (2009).
[2] H. E. Parge, R. A. Hallewell, and J. A. Tainer, Proceedings of the National Academy of Sciences **89**, 6109 (1992).
[3] R. Williams, Journal of molecular catalysis **30**, 1 (1985).
[4] A. Kermagoret, R. N. Kerber, M. P. Conley, E. Callens, P. Florian, D. Massiot, F. Delbecq, X. Rozanska, C. Copéret, and P. Sautet, Journal of Catalysis **313**, 46 (2014).
[5] C. Copéret, Chemical reviews **110**, 656 (2009).
[6] M. S. Whittingham, Science **192**, 1126 (1976).
[7] M. S. Whittingham, Chemical reviews **104**, 4271 (2004).
[8] A. . K. Padhi, K. Nanjundaswamy, and J. B. d. Goodenough, Journal of the electrochemical society **144**, 1188 (1997).
[9] F. Blanc, C. Copéret, A. Lesage, and L. Emsley, Chemical Society Reviews **37**, 518 (2008).
[10] I. Bertini, C. Luchinat, G. Parigi, and R. Pierattelli, Dalton Transactions , 3782 (2008).
[11] M. J. Knight, A. J. Pell, I. Bertini, I. C. Felli, L. Gonnelli, R. Pierattelli, T. Herrmann, L. Emsley, and G. Pintacuda, Proceedings of the National Academy of Sciences **109**, 11095 (2012).
[12] D. S. Middlemiss, A. J. Ilott, R. J. Clément, F. C. Strobridge, and C. P. Grey, Chemistry of Materials **25**, 1723

(2013).
[13] D. Carlier, M. Ménétrier, C. P. Grey, C. Delmas, and G. Ceder, Physcal Review B **67**, 174103 (2003).
[14] H. M. McConnell and D. B. Chesnut, The Journal of Chemical Physics **28**, 107 (1958).
[15] H. M. McConnell and R. E. Robertson, The Journal of Chemical Physics **29**, 1361 (1958).
[16] R. J. Kurland and B. R. McGarvey, Journal of Magnetic Resonance **2**, 286 (1970).
[17] M. Kaupp and F. H. Köhler, Coordination Chemistry Reviews **253**, 2376 (2009).
[18] C. P. Grey, , and N. Dupré, Chemical Reviews **104**, 4493 (2004).
[19] M. Kaupp, M. Bühl, and V. G. Malkin, *Calculation of NMR and EPR parameters: theory and applications - Chapter 20 by S. Moon and S. Patchkovskii* (John Wiley & Sons, 2006).
[20] T. O. Pennanen and J. Vaara, Physical review letters **100**, 133002 (2008).
[21] J. Vaara, S. A. Rouf, and J. Mares, Journal of chemical theory and computation **11**, 4840 (2015).
[22] W. Van den Heuvel and A. Soncini, Physical review letters **109**, 073001 (2012).
[23] P. Hrobárik, R. Reviakine, A. V. Arbuznikov, O. L. Malkina, V. G. Malkin, F. H. Köhler, and M. Kaupp, The Journal of chemical physics **126**, 024107 (2007).
[24] S. A. Rouf, J. Mares, and J. Vaara, Journal of chemical theory and computation **11**, 1683 (2015).
[25] H. Liimatainen, T. O. Pennanen, and J. Vaara, Canadian Journal of Chemistry **87**, 954 (2009).
[26] B. Martin and J. Autschbach, Physical Chemistry Chemical Physics (2016).
[27] B. Martin and J. Autschbach, The Journal of chemical physics **142**, 054108 (2015).
[28] J. Novotny, M. Sojka, S. Komorovsky, M. Necas, and R. Marek, Journal of the American Chemical Society **138**, 8432 (2016).
[29] J. Kim, D. S. Middlemiss, N. A. Chernova, B. Y. Zhu, C. Masquelier, and C. P. Grey, Journal of the American Chemical Society **132**, 16825 (2010).
[30] G. Mali, C. Sirisopanaporn, C. Masquelier, D. Hanzel, and R. Dominko, Chemistry of Materials **23**, 2735 (2011).
[31] A. . K. Padhi, K. Nanjundaswamy, and J. Goodenough, Journal of the electrochemical society **144**, 1188 (1997).
[32] M. S. Whittingham, Chemical reviews **114**, 11414 (2014).
[33] M. C. Tucker, M. M. Doeff, T. J. Richardson, R. Finones, E. J. Cairns, and J. A. Reimer, Journal of the American Chemical Society **124**, 3832 (2002).
[34] S. Wilcke, Y.-J. Lee, E. Cairns, and J. Reimer, Applied Magnetic Resonance **32**, 547 (2007).
[35] In this work the effects of Zero Field Splitting (ZFS) are neglected. This approximation is discussed in the S.I.
[36] I. Bertini, C. Luchinat, and G. Parigi, Progress in Nuclear Magnetic Resonance Spectroscopy **40**, 249 (2002).
[37] R. J. Clément, A. J. Pell, D. S. Middlemiss, F. C. Strobridge, J. K. Miller, M. S. Whittingham, L. Emsley, C. P. Grey, and G. Pintacuda, Journal of the American Chemical Society **134**, 17178 (2012).
[38] C. Chazel, M. Ménétrier, L. Croguennec, and C. Delmas, Magnetic Resonance in Chemistry **43**, 849 (2005).
[39] M. I. Aroyo, J. M. Perez-Mato, C. Capillas, E. Kroumova, S. Ivantchev, G. Madariaga, A. Kirov, and H. Wondratschek, Zeitschrift für Kristallographie **221**, 15 (2006).
[40] M. I. Aroyo, A. Kirov, C. Capillas, J. Perez-Mato, and H. Wondratschek, Acta Crystallographica Section A: Foundations of Crystallography **62**, 115 (2006).
[41] M. Aroyo, J. Perez-Mato, D. Orobengoa, E. Tasci, G. De La Flor, and A. Kirov, Bulg. Chem. Commun **43**, 183 (2011).
[42] F. Mobbs and D. Collison, *Electron Paramagnetic Resonance of d Transition Metal Compounds, Vol. 16* (Elsevier, Amsterdam, 1992).
[43] J. E. Harriman, *Theoretical Foundations of Electron Spin Resonance* (Academic Press INC., 1978).
[44] R. C. Powell, *Symmetry, Group Theory, and the Physical Properties of Crystals* (Springer, 2010).
[45] A. Abragam and B. Bleaney, *Electron paramagnetic resonance of transition ions* (Oxford University Press, 2012).
[46] C. J. Pickard and F. Mauri, Physical Review B **63**, 245101 (2001).
[47] C. J. Pickard and F. Mauri, Physical review letters **88**, 086403 (2002).
[48] C. Remenyi, R. Reviakine, A. V. Arbuznikov, J. Vaara, and M. Kaupp, The Journal of Physical Chemistry A **108**, 5026 (2004).
[49] C. Remenyi, R. Reviakine, and M. Kaupp, The Journal of Physical Chemistry B **111**, 8290 (2007).
[50] R. Dovesi, R. Orlando, B. Civalleri, C. Roetti, V. R. Saunders, and C. M. Zicovich-Wilson, Zeitschrift für Kristallographie **220**, 571 (2005).
[51] R. Dovesi, V. R. Saunders, C. Roetti, R. Orlando, C. M. Zicovitch-Wilson, F. Pascale, B. Civarelli, K. Doll, N. M. Harrison, I. J. Bush, P. D'Arco, and M. Llunell, *CRYSTAL09 User's Manual*, Vol. Torino (Università di Torino, 2009).
[52] P. Giannozzi, S. Baroni, N. Bonini, M. Calandra, R. Car, C. Cavazzoni, D. Ceresoli, G. L. Chiarotti, M. Cococcioni, I. Dabo, A. Dal Corso, S. de Gironcoli, S. Fabris, G. Fratesi, R. Gebauer, U. Gerstmann, C. Gougoussis, A. Kokalj, M. Lazzeri, L. Martin-Samos, N. Marzari, F. Mauri, R. Mazzarello, S. Paolini, A. Pasquarello, L. Paulatto, C. Sbraccia, S. Scandolo, G. Sclauzero, A. P. Seitsonen, A. Smogunov, P. Umari, and R. M. Wentzcovitch, Journal of Physics: Condensed Matter **21** (2009).
[53] F. Corà, M. Alfredsson, G. Mallia, D. S. Middlemiss, W. C. Mackrodt, R. Dovesi, and R. Orlando, in *Principles and Applications of Density Functional Theory in Inorganic Chemistry II* (Springer, 2004) pp. 171–232.
[54] J. P. Perdew, K. Burke, and M. Ernzerhof, Physical review letters **77**, 3865 (1996).
[55] C. Adamo and V. Barone, The Journal of chemical physics **110**, 6158 (1999).
[56] M. Munzarová and M. Kaupp, The Journal of Physical Chemistry A **103**, 9966 (1999).
[57] M. Kaupp, R. Reviakine, O. L. Malkina, A. Arbuznikov, B. Schimmelpfennig, and V. G. Malkin, Journal of computational chemistry **23**, 794 (2002).
[58] P. E. Blöchl, Physical Review B **50**, 17953 (1994).
[59] V. I. Anisimov, J. Zaanen, and O. K. Andersen, Physical Review B **44**, 943 (1991).
[60] P. Verma and D. G. Truhlar, Theoretical Chemistry Accounts **135**, 1 (2016).
[61] F. Zhou, M. Cococcioni, C. A. Marianetti, D. Morgan, and G. Ceder, Physical Review B **70**, 235121 (2004).
[62] F. Zhou, M. Cococcioni, K. Kang, and G. Ceder, Electrochemistry communications **6**, 1144 (2004).

[63] F. Zhou, C. Marianetti, M. Cococcioni, D. Morgan, and G. Ceder, Physical review B **69**, 201101 (2004).
[64] G. Hautier, A. Jain, S. P. Ong, B. Kang, C. Moore, R. Doe, and G. Ceder, Chemistry of Materials **23**, 3495 (2011).
[65] H. Xiang, C. Lee, H.-J. Koo, X. Gong, and M.-H. Whangbo, Dalton Transactions **42**, 823 (2013).
[66] S. Dudarev, G. Botton, S. Savrasov, C. Humphreys, and A. Sutton, Physical Review B **57**, 1505 (1998).
[67] O. Garcia-Moreno, M. Alvarez-Vega, F. Garcia-Alvarado, J. Garcia-Jaca, J. Gallardo-Amores, M. Sanjuán, and U. Amador, Chemistry of materials **13**, 1570 (2001).
[68] G. Rousse, J. Rodriguez-Carvajal, S. Patoux, and C. Masquelier, Chemistry of materials **15**, 4082 (2003).
[69] F. Kubel, Zeitschrift fur Kristallographie - New Crystal Structures **209**, 755 (1994).
[70] R. K. Harris, E. D. Becker, S. M. C. De Menezes, P. Granger, R. E. Hoffman, and K. W. Zilm, Magnetic Resonance in Chemistry **46**, 582 (2008).
[71] L. Enciso-Maldonado, M. S. Dyer, M. D. Jones, M. Li, J. L. Payne, M. J. Pitcher, M. K. Omir, J. B. Claridge, F. Blanc, and M. J. Rosseinsky, Chemistry of Materials **27**, 2074 (2015).
[72] V. Koleva, E. Zhecheva, and R. Stoyanova, Dalton Transactions **40**, 7385 (2011).
[73] N. Wizent, G. Behr, F. Lipps, I. Hellmann, R. Klingeler, V. Kataev, W. Löser, N. Sato, and B. Büchner, Journal of Crystal Growth **311**, 1273 (2009).
[74] V. Singh, Y. Gershinsky, M. Kosa, M. Dixit, D. Zitoun, and D. T. Major, Physical Chemistry Chemical Physics **17**, 31202 (2015).
[75] G. Liang, K. Park, J. Li, R. E. Benson, D. Vaknin, J. T. Markert, and M. C. Croft, Physical Review B **77**, 064414 (2008).
[76] D. Vaknin, J. Zarestky, L. Miller, J.-P. Rivera, and H. Schmid, Physical Review B **65**, 224414 (2002).
[77] S.-H. Baek, R. Klingeler, C. Neef, C. Koo, B. Büchner, and H.-J. Grafe, Physical Review B **89**, 134424 (2014).
[78] A. Goni, L. Lezama, G. Barberis, J. Pizarro, M. Arriortua, and T. Rojo, Journal of magnetism and magnetic materials **164**, 251 (1996).
[79] R. Boča, Coordination chemistry reviews **248**, 757 (2004).
[80] H. Jiang, R. I. Gomez-Abal, P. Rinke, and M. Scheffler, Physical Review B **82**, 045108 (2010).
[81] A. Castets, D. Carlier, Y. Zhang, F. Boucher, N. Marx, L. Croguennec, and M. Ménétrier, The Journal of Physical Chemistry C **115**, 16234 (2011).
[82] F. Zhou, K. Kang, T. Maxisch, G. Ceder, and D. Morgan, Solid State Communications **132**, 181 (2004).
[83] M. Forti, P. Alonso, P. Gargano, and G. Rubiolo, Procedia Materials Science **1**, 230 (2012).
[84] A. Jena and B. Nanda, Scientific reports **6** (2016).
[85] O. Le Bacq, A. Pasturel, and O. Bengone, Physical Review B **69**, 245107 (2004).
[86] F. Zhou, M. Cococcioni, C. A. Marianetti, D. Morgan, and G. Ceder, Physical Review B **70**, 235121 (2004).
[87] D. Massiot, F. Fayon, M. Capron, I. King, S. Le Calvé, B. Alonso, J.-O. Durand, B. Bujoli, Z. Gan, and G. Hoatson, Magnetic Resonance in Chemistry **40**, 70 (2002).
[88] L. Drain, Proceedings of the Physical Society **80**, 1380 (1962).